J. Fluid Mech. (2007), *vol.* 585, *pp.* 281–304.
doi:10.1017/S0022112007006647 Printed in the United Kingdom

The forced response of choked nozzles and supersonic diffusers

WILLIAM H. MOASE[1], MICHAEL J. BREAR[1] AND CHRIS MANZIE[1]

[1]Department of Mechanical and Manufacturing Engineering, University of Melbourne, VIC, 3010, Australia

(Received 19 May 2006 and in revised form 26 March 2007)

The response of choked nozzles and supersonic diffusers to one-dimensional flow perturbations is investigated. Following previous arguments in the literature, small flow perturbations in a duct of spatially linear steady velocity distribution are determined by solution of a hyper-geometric differential equation. A set of boundary conditions is then developed that extends the existing work to a nozzle of arbitrary geometry. This analysis accommodates the motion of a plane shock wave and makes no assumption about the nozzle compactness. Numerical simulations of the unsteady, quasi-one-dimensional Euler equations are performed to validate this analysis and also to indicate the conditions under which the perturbations remain approximately linear.

The nonlinear response of compact choked nozzles and supersonic diffusers is also investigated. Simple analyses are performed to determine the reflected and transmitted waveforms, as well as conditions for unchoke, 'over-choke' and unstart. This analysis is also supported with results from numerical simulations of the Euler equations.

1. Introduction

Choked nozzles and supersonic diffusers appear in many engineering devices, such as aircraft, gas turbines, ramjets and wind tunnels. In such cases, it is common for pressure and entropy fluctuations to interact with the geometry and shocks, occasionally with undesirable consequences. For example, atmospheric disturbances enter the supersonic diffuser of a ramjet in flight, and can result in the expulsion of a normal shock from the inlet. This process, known as 'unstart', causes a sudden reduction in thrust (see Mayer & Paynter 1995). In the premixed combustor of a gas turbine, the acoustic and entropic disturbances produced by flame motion interact with a choked outlet nozzle, resulting in a reflected pressure wave. This pressure wave travels upstream and interacts with the flame, causing further flame motion. Depending on the exact response of the choked outlet nozzle to the perturbations, the feedback provided by the nozzle may result in 'thermoacoustic instability', which can lead to blow-out of the flame, or sound pressure levels large enough to damage the gas turbine (see Dowling & Hubbard 2000). It is therefore important to understand the response of a choked nozzle or supersonic diffuser to excitation by incident disturbances.

Tsien (1952) provided the first detailed analysis of the forced response of a quasi-one-dimensional choked nozzle. He analytically determined the fractional mass flow perturbation at the nozzle entrance as a response to perturbations in the fractional

pressure. For a choked nozzle with a spatially linear steady velocity profile, he was able to reduce the linearized mass, momentum, and energy equations to a hyper-geometric differential equation. Because he was only interested in the fluid behaviour at the entrance to the nozzle, the effect of a shock downstream of the throat was ignored since small perturbations in the supersonic region downstream of the throat cannot travel upstream. Because of computational limitations, Tsien (1952) only studied the high- and low-frequency limits of the response.

Marble & Candel (1977) extended the analysis of Tsien (1952) to study the transmission and reflection coefficients of compact and finite-length choked nozzles. Their work focused on the influence of entropy disturbances (sometimes called convected 'hot spots') but could also be used to find the response to acoustic excitation. They showed that a choked outlet nozzle not only reflected downstream travelling pressure waves but also acted as a source of sound for incident entropy disturbance. They were able to overcome the computational limitations faced by Tsien (1952) and studied the frequency dependence of the nozzle, but they still assumed that the nozzle geometry was such that the steady velocity distribution was linear, and that no shock existed in the nozzle. Their discussion of the effect of normal shocks was limited to a brief study of a compact nozzle with a shock downstream where the only excitation was an entropy disturbance.

Culick & Rogers (1983) provided an analytical technique for determining the frequency-dependent acoustic impedance downstream of a shock wave in a ramjet engine. Their analysis was based on solving the unsteady Rankine–Hugoniot equations across the shock whilst simultaneously considering the shock motion. They did not consider the influence of the area change throughout the nozzle, and were concerned only with the influence of acoustic disturbances from downstream.

Stow, Dowling & Hynes (2002) provided an extension to the analysis of Culick & Rogers (1983) by developing a relationship between the fractional pressure, velocity and density perturbations and the shock displacement. This provided a means of determining the unsteady entropy generation at the shock. Since they were not concerned with the transmission of disturbances through the nozzle, they did not consider the effect of perturbations entering the shock from upstream. Although their result was true for arbitrary forcing frequency, they made the assumption that the frequency was zero when applying it to the case of a choked inlet nozzle. This final result was therefore only valid for compact nozzles. Stow *et al.* (2002) also studied the reflection coefficient of choked outlet nozzles with arbitrary geometries, although since their analysis was to first order in the excitation frequency, it was only valid in the low frequency limit.

It therefore appears that a comprehensive study of the frequency response of choked nozzles and supersonic diffusers containing shocks is yet to be performed. Previous studies appear to assume one or more of compactness, low forcing frequency, shock-free flow or ignore area changes. The work presented in § 2 therefore builds on the models of Marble & Candel (1977) and Stow *et al.* (2002) to develop a model that predicts the one-dimensional frequency response of choked nozzles and supersonic diffusers containing shocks. Excitation by both incident pressure and entropy waves are considered, as well as the acoustic and entropic response. The model is valid for arbitrary excitation frequency and considers planar shock motion. The model is also applicable to any nozzle geometry as long as the steady velocity distribution can be approximated as piecewise linear. Analyses of the nonlinear response as well as conditions for unchoking, unstarting and 'over-choking' of compact choked nozzles and compact supersonic diffusers are also presented.

Section 3 describes a numerical solution of the quasi-one-dimensional Euler equations. In § 4, this solver is applied to a range of choked nozzle and supersonic diffuser geometries under various forms of excitation. The results of these simulations are compared to the analytical results presented in § 2, and agree favourably. The numerical solver is also used to study nonlinear, non-compact phenomena to which the analytical results do not apply.

2. Theory

2.1. *Equations of motion*

Consider the quasi-one-dimensional Euler equations applied to a calorifically perfect, ideal gas,

$$\frac{\partial}{\partial t}(\rho A) + \frac{\partial}{\partial x}(\rho u A) = 0, \tag{2.1a}$$

$$\frac{\partial}{\partial t}(\rho u A) + \frac{\partial}{\partial x}([p + \rho u^2]A) = p\frac{\mathrm{d}A}{\mathrm{d}x}, \tag{2.1b}$$

$$\frac{\partial}{\partial t}\left(\left[\frac{p}{\gamma - 1} + \tfrac{1}{2}\rho u^2\right]A\right) + \frac{\partial}{\partial x}\left(\left[\frac{\gamma p}{\gamma - 1} + \tfrac{1}{2}\rho u^2\right]uA\right) = 0, \tag{2.1c}$$

where u is velocity, p is pressure, ρ is density, A is the cross-sectional area of the duct, and γ is the ratio of specific heats ($\gamma = 1.4$ for all presented calculations). If the cross-sectional area of the duct is constant, these equations of motion can be linearized in the perturbation quantities to obtain

$$\frac{\partial p^+}{\partial t} + (\bar{u} + \bar{c})\frac{\partial p^+}{\partial x} = 0, \tag{2.2a}$$

$$\frac{\partial p^-}{\partial t} + (\bar{u} - \bar{c})\frac{\partial p^-}{\partial x} = 0, \tag{2.2b}$$

$$\left\{\frac{\partial}{\partial t} + \bar{u}\frac{\partial}{\partial x}\right\}\left(\frac{s'}{c_p}\right) = 0, \tag{2.2c}$$

where

$$p^+ = \frac{p'}{\gamma\bar{p}} + \frac{u'}{\bar{c}}, \qquad p^- = \frac{p'}{\gamma\bar{p}} - \frac{u'}{\bar{c}}, \qquad \frac{s'}{c_p} = \frac{p'}{\gamma\bar{p}} - \frac{\rho'}{\bar{\rho}}, \tag{2.3a–c}$$

c is the speed of sound, s' is the entropy perturbation, c_p is the specific heat at constant pressure, $\bar{(\,)}$ represents steady flow quantities and $(\,)'$ represents perturbations about the steady flow. Equations (2.2*a*)–(2.2*c*) show that the system is composed of three perturbations: acoustic waves p^+ and p^- travelling downstream and upstream respectively at the speed of sound with respect to the steady flow, and a convected entropy perturbation s'/c_p. Thus any section within a quasi-one-dimensional flow has a number of disturbances entering and exiting it. For linear harmonic solutions, the reflection and transmission coefficients are the transfer functions of the entering disturbances to the exiting disturbances.

2.2. *Dynamic shock relations*

This subsection develops relations that describe the response of a normal shock wave to acoustic and entropic excitation. The development of these shock relations follows the same arguments as those given by Stow *et al.* (2002); however, because the transmission behaviour of the nozzle is also of interest, the effects of perturbations

entering the shock from upstream are considered. To first order in the perturbation quantities, the speed of sound at the shock is

$$c_{1,sh}(x_s) = c_1(x_s) = \bar{c}_1(\bar{x}_s) + c_1'(\bar{x}_s) + x_s' \left(\frac{\mathrm{d}\bar{c}_1}{\mathrm{d}x}\right)_{x_s=\bar{x}_s}, \tag{2.4}$$

where c is the speed of sound, x_s is the shock location, the subscript $(\,)_{sh}$ denotes quantities taken in the shock frame of reference, and the subscript $(\,)_1$ denotes quantities measured on the upstream side of the shock. Since the steady stagnation speed of sound is conserved throughout the domain,

$$\frac{\mathrm{d}\bar{c}}{\mathrm{d}x} = -\frac{(\gamma-1)}{2}\bar{M}\frac{\mathrm{d}\bar{u}}{\mathrm{d}x}, \tag{2.5}$$

for adiabatic flow, where M is the Mach number. Substituting (2.5) into (2.4) yields

$$\frac{c_{1,sh}}{\bar{c}_1} = 1 + \frac{c_1'}{\bar{c}_1} - x_s'\frac{(\gamma-1)}{2}\frac{\bar{M}_1^2}{\bar{u}_1}\frac{\mathrm{d}\bar{u}_1}{\mathrm{d}x}. \tag{2.6}$$

Similarly, assuming that the disturbances are harmonic with time dependence $\exp(\mathrm{i}\omega t)$,

$$u_{1,sh} = u_1 - \frac{\mathrm{d}x_s}{\mathrm{d}t} = \bar{u}_1 + u_1' + x_s'\left(\frac{\mathrm{d}\bar{u}_1}{\mathrm{d}x} - \mathrm{i}\omega\right). \tag{2.7}$$

The linearization given in (2.4) is only valid for infinitesimal positive and negative perturbations in the shock location if

$$\left(\frac{\mathrm{d}\bar{c}_1}{\mathrm{d}x}\right)_{x_s=\bar{x}_s-\epsilon} = \left(\frac{\mathrm{d}\bar{c}_1}{\mathrm{d}x}\right)_{x_s=\bar{x}_s+\epsilon}, \tag{2.8}$$

where ϵ is an infinitesimally small distance. This can be ensured if $\mathrm{d}A/\mathrm{d}x$ is continuous at the steady shock location. In conjunction with the area–Mach number relation for isentropic flow, this requirement can be expressed as

$$\frac{1}{A}\frac{\mathrm{d}A}{\mathrm{d}x} = \frac{\bar{M}_1^2-1}{\bar{M}_1\left(1+\frac{1}{2}(\gamma-1)\bar{M}_1^2\right)}\frac{\mathrm{d}\bar{M}_1}{\mathrm{d}x} = \frac{\bar{M}_2^2-1}{\bar{M}_2\left(1+\frac{1}{2}(\gamma-1)\bar{M}_2^2\right)}\frac{\mathrm{d}\bar{M}_2}{\mathrm{d}x}, \tag{2.9}$$

where $(\,)_2$ denotes quantities measured on the downstream side of the shock. Substitution of (2.5) into (2.9) yields

$$\frac{\mathrm{d}\bar{u}_2}{\mathrm{d}x} = \frac{\bar{u}_2}{\bar{u}_1}\frac{\bar{M}_1^2-1}{\bar{M}_2^2-1}\frac{\mathrm{d}\bar{u}_1}{\mathrm{d}x}. \tag{2.10}$$

Now define $\Omega = \omega/(\mathrm{d}\bar{u}/\mathrm{d}x)$ as the non-dimensional frequency. The value of $|\Omega|$ can be thought of as a measure of the acoustic compactness of a contraction or expansion. Substituting (2.10) into (2.7) gives

$$\frac{u_{1,sh}}{\bar{u}_1} = 1 + \frac{u_1'}{\bar{u}_1} + \frac{x_s'}{\bar{u}_1}\frac{\mathrm{d}\bar{u}_1}{\mathrm{d}x}\left(1 - \frac{\bar{u}_2}{\bar{u}_1}\frac{\bar{M}_1^2-1}{\bar{M}_2^2-1}\mathrm{i}\Omega_2\right). \tag{2.11}$$

Dividing (2.11) by (2.6) gives

$$\frac{M_{1,sh}}{\bar{M}_1} = 1 + \frac{M_1'}{\bar{M}_1} + \frac{x_s'}{\bar{u}_1}\frac{\mathrm{d}\bar{u}_1}{\mathrm{d}x}\left(1 + \frac{\gamma-1}{2}\bar{M}_1^2 - \frac{\bar{u}_2}{\bar{u}_1}\frac{\bar{M}_1^2-1}{\bar{M}_2^2-1}\mathrm{i}\Omega_2\right). \tag{2.12}$$

The Rankine–Hugoniot shock relation for velocity states that

$$\frac{u_{1,sh}}{u_{2,sh}} = \frac{(\gamma+1)M_{1,sh}^2}{2+(\gamma-1)M_{1,sh}^2}. \tag{2.13}$$

Substituting (2.11) and (2.12) into (2.13) gives

$$\frac{u_{2,sh}}{\bar{u}_2} = 1 - \frac{x_s'}{\bar{u}_1}\frac{\mathrm{d}\bar{u}_1}{\mathrm{d}x}\left[1 + \mathrm{i}\Omega_2\frac{\bar{u}_2}{\bar{u}_1}\frac{2-(\gamma-1)\bar{M}_1^2}{(\gamma+1)\bar{M}_2^2}\right] + \frac{2}{2-(\gamma+1)\bar{M}_1^2}\left[\gamma\frac{p_1'}{\gamma\bar{p}_1} - \frac{\rho_1'}{\bar{\rho}_1} - \left(1 - \frac{\gamma-1}{2}\bar{M}_1^2\right)\frac{u_1'}{\bar{u}_1}\right]. \tag{2.14}$$

It is also true that

$$u_{2,sh} = u_2 - \frac{\mathrm{d}x_s}{\mathrm{d}t} = \bar{u}_2 + u_2' + x_s'\left(\frac{\mathrm{d}\bar{u}_2}{\mathrm{d}x} - \mathrm{i}\omega\right), \tag{2.15}$$

which after further manipulation yields

$$\frac{u_{2,sh}}{\bar{u}_2} = 1 + \frac{u_2'}{\bar{u}_2} - \frac{x_s'}{\bar{u}_1}\frac{\mathrm{d}\bar{u}_1}{\mathrm{d}x}\frac{\bar{M}_1^2}{\bar{M}_2^2}\frac{\bar{u}_2}{\bar{u}_1}(1 - \mathrm{i}\Omega_2). \tag{2.16}$$

Substituting (2.16) into (2.14) gives

$$\frac{u_2'}{\bar{u}_2} = \frac{2x_s'}{(\gamma+1)\bar{u}_1}\frac{\mathrm{d}\bar{u}_1}{\mathrm{d}x}E_u + \frac{2}{2+(\gamma-1)\bar{M}_1^2}F_u, \tag{2.17}$$

where

$$E_u = -\gamma(1-\bar{M}_1^2) - \frac{\bar{u}_2}{\bar{u}_1}\frac{1+\bar{M}_1^2}{\bar{M}_2^2}\mathrm{i}\Omega_2, \quad F_u = \gamma\frac{p_1'}{\gamma\bar{p}_1} - \frac{\rho_1'}{\bar{\rho}_1} - \left(1 - \frac{\gamma-1}{2}\bar{M}_1^2\right)\frac{u_1'}{\bar{u}_1}.$$

Starting with the Rankine–Hugoniot shock relations for pressure and density, similar arguments can be applied to show that on the downstream side of the shock

$$\frac{p_2'}{\gamma\bar{p}_2} = \frac{2x_s'}{(\gamma+1)\bar{u}_1}\frac{\mathrm{d}\bar{u}_1}{\mathrm{d}x}E_p + \frac{2}{2+(\gamma-1)\bar{M}_1^2}F_p, \tag{2.18}$$

$$\frac{\rho_2'}{\bar{\rho}_2} = \frac{2x_s'}{(\gamma+1)\bar{u}_1}\frac{\mathrm{d}\bar{u}_1}{\mathrm{d}x}E_\rho + \frac{2}{2+(\gamma-1)\bar{M}_1^2}F_\rho, \tag{2.19}$$

where

$$E_p = \frac{(1+\gamma^2)\bar{M}_1^2 + \gamma - 1}{2\gamma\bar{M}_1^2 - \gamma + 1}\left(1 - \bar{M}_1^2\right) + 2\frac{\bar{u}_2}{\bar{u}_1}\bar{M}_1^2\mathrm{i}\Omega_2,$$

$$F_p = \bar{M}_2^2\left(\frac{1-\gamma}{2}\frac{p_1'}{\gamma\bar{p}_1} + \bar{M}_1^2\frac{\rho_1'}{\bar{\rho}_1} + 2\bar{M}_1^2\frac{u_1'}{\bar{u}_1}\right),$$

$$E_\rho = \gamma\left(1-\bar{M}_1^2\right) + \frac{2\bar{u}_2}{\bar{u}_1\bar{M}_2^2}\mathrm{i}\Omega_2, \quad F_\rho = -\gamma\frac{p_1'}{\gamma\bar{p}_1} + \left(2 + \frac{\gamma-1}{2}\bar{M}_1^2\right)\frac{\rho_1'}{\bar{\rho}_1} + 2\frac{u_1'}{\bar{u}_1}.$$

At the shock there are four incoming waves (p_1^+, p_1^-, s_1'/c_p and p_2^-) and two outgoing waves (p_2^+ and s_2'/c_p). Only two equations are therefore required to solve for these outgoing waves, and to describe fully the linear reflection and transmission of the shock. Two such equations can be found by cancelling x_s' out of (2.17)–(2.19),

$$\frac{u_2'}{\bar{u}_2} = \frac{p_2'}{\gamma\bar{p}_2}\frac{E_u}{E_p} + \frac{F_u - F_pE_u/E_p}{1 + \frac{1}{2}(\gamma-1)\bar{M}_1^2}, \tag{2.20a}$$

$$\frac{s_2'}{c_p} = \frac{p_2'}{\gamma\bar{p}_2}\left[1 - \frac{E_\rho}{E_p}\right] - \frac{F_\rho - F_pE_\rho/E_p}{1 + \frac{1}{2}(\gamma-1)\bar{M}_1^2}. \tag{2.20b}$$

2.3. *Transmission and reflection coefficients for finite-length choked nozzles*

It is common to consider a linear steady velocity distribution in the study of transmission and reflection of nozzles (see Tsien 1952; Marble & Candel 1977) because this facilitates analytical solution. Such a velocity profile is clearly insufficient to describe a shock, so a piecewise linear steady velocity profile will be considered instead. In order to find an analytic solution for the acoustics in a nozzle with a piecewise linear steady velocity distribution, it is necessary first to find a general analytic solution for the acoustics in a region of linear velocity distribution, and then specify appropriate boundary conditions to describe the interaction of connected regions. This approach is outlined in the next three sub-subsections.

2.3.1. *Analytic solution of perturbations in a region of linear steady velocity profile*

Marble & Candel (1977) reduce the description of the flow perturbations in a section of duct with a linearly distributed steady velocity to a hyper-geometric differential equation. They start by linearizing (2.1*a*)–(2.1*c*) in the perturbation quantities to obtain (2.2*c*),

$$\left\{\frac{\partial}{\partial t}+\bar{u}\frac{\partial}{\partial x}\right\}\left(\frac{p'}{\gamma\bar{p}}\right)+\bar{u}\frac{\partial}{\partial x}\left(\frac{u'}{\bar{u}}\right)=0, \quad (2.21)$$

$$\left\{\frac{\partial}{\partial t}+\bar{u}\frac{\partial}{\partial x}\right\}\left(\frac{u'}{\bar{u}}\right)+\frac{\bar{c}^2}{\bar{u}}\frac{\partial}{\partial x}\left(\frac{u'}{\bar{u}}\right)+\left[2\frac{u'}{\bar{u}}-(\gamma-1)\frac{p'}{\gamma\bar{p}}-\frac{s'}{c_p}\right]\frac{\mathrm{d}\bar{u}}{\mathrm{d}x}=0. \quad (2.22)$$

Take the origin of the x-coordinate system to be the location at which the steady velocity is zero. This origin will not be located within the region being studied, but can be found by extrapolation of the steady velocity profile. Let the subscript $(\,)_*$ denote quantities taken at the location at which the steady flow is choked (again, this might not be located within the region being studied), i.e. $\bar{u}_*=\bar{c}_*$ at x_*. Therefore $\bar{u}(x)=x\bar{c}_*/x_*$. Let dimensionless time and position be defined as $\tau=t\bar{c}_*/x_*$ and $\xi=(x/x_*)^2$ respectively. Marble & Candel (1977) then transform (2.2*c*), (2.21) and (2.22) into dimensionless terms to obtain

$$\left\{\frac{\partial}{\partial\tau}+2\xi\frac{\partial}{\partial\xi}\right\}\left(\frac{p'}{\gamma\bar{p}}\right)+2\xi\frac{\partial}{\partial\xi}\left(\frac{u'}{\bar{u}}\right)=0, \quad (2.23a)$$

$$\left\{\frac{\partial}{\partial\tau}+2\xi\frac{\partial}{\partial\xi}\right\}\left(\frac{u'}{\bar{u}}\right)+\left[\frac{\gamma+1}{\xi}-\gamma+1\right]\xi\frac{\partial}{\partial\xi}\left(\frac{p'}{\gamma\bar{p}}\right)+2\frac{u'}{\bar{u}}-(\gamma-1)\frac{p'}{\gamma\bar{p}}=\frac{s'}{c_p}, \quad (2.23b)$$

$$\left\{\frac{\partial}{\partial\tau}+2\xi\frac{\partial}{\partial\xi}\right\}\left(\frac{s'}{c_p}\right)=0. \quad (2.23c)$$

Finally Marble & Candel (1977) assume that the disturbances have time dependence $\exp(\mathrm{i}\Omega\tau)$, and let $p'/(\gamma\bar{p})=P(\xi)\exp(\mathrm{i}\Omega\tau)$, $u'/\bar{u}=U(\xi)\exp(\mathrm{i}\Omega\tau)$ and $s'/c_p=\sigma(\xi)\exp(\mathrm{i}\Omega\tau)$ to gain

$$\sigma=\sigma_r\left(\frac{\xi}{\xi_r}\right)^{-\mathrm{i}\Omega/2}, \quad (2.24a)$$

$$\xi(1-\xi)\frac{\mathrm{d}^2P}{\mathrm{d}\xi^2}-2\frac{\gamma+1+\mathrm{i}\Omega}{\gamma+1}\xi\frac{\mathrm{d}P}{\mathrm{d}\xi}-\frac{\mathrm{i}\Omega(2+\mathrm{i}\Omega)}{2(\gamma+1)}P=\frac{-\mathrm{i}\Omega\sigma}{2(\gamma+1)}, \quad (2.24b)$$

$$(2+\mathrm{i}\Omega)U=-(\gamma+1)(1-\xi)\frac{\mathrm{d}P}{\mathrm{d}\xi}+(\gamma-1+\mathrm{i}\Omega)P+\sigma, \quad (2.24c)$$

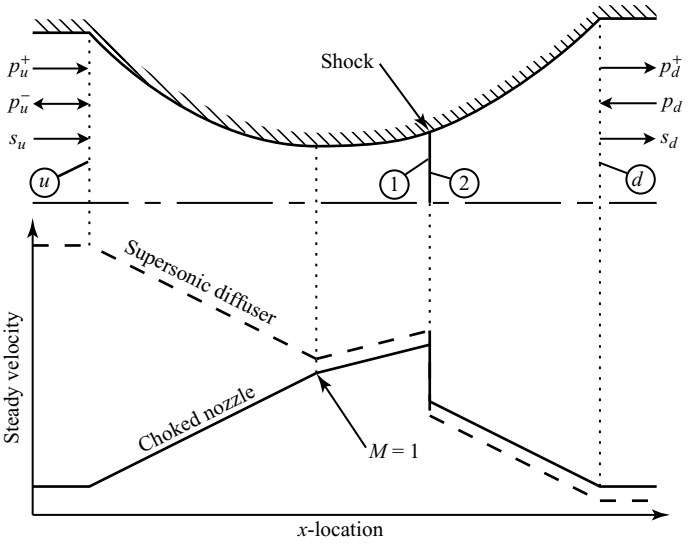

FIGURE 1. Geometry of nozzle and steady velocity distribution.

where the subscript $(\,)_r$ refers to the value of a property taken at a reference location. Equation (2.24*b*) is hyper-geometric. Solutions based on polynomials of the variable $1-\xi$ will be considered here since these series will converge for $0 < \xi < 2$, which will at least allow the study of all flows with $M < \sqrt{4/(3-\gamma)}$. Although not discussed in this paper, when analysing higher Mach number flows, it should be a relatively simple matter to model regions containing only supersonic flow with hyper-geometric solutions in the variable ξ^{-1}. However, the solution considered here is

$$P = \sigma_r P_p + a_0 P_{h1} + b_0 P_{h2}, \tag{2.25}$$

where

$$P_p = \frac{-\mathrm{i}\Omega \xi_r^{\,\mathrm{i}\Omega/2}}{2(\gamma+1)} \sum_{n=0}^{\infty} c_n (1-\xi)^{n+1}, \qquad P_{h1} = \sum_{n=0}^{\infty} \frac{a^{(n)} b^{(n)}}{n!(1+a+b)^{(n)}} (1-\xi)^n,$$

$$P_{h2} = \sum_{n=0}^{\infty} \frac{(-a)^{(n)}(-b)^{(n)}}{n!(1-a-b)^{(n)}} (1-\xi)^{n-a-b},$$

$$c_0 = \frac{1}{1+a+b}, \quad c_n = \frac{c_{n-1}(n+a)(n+b)n! + \left(1-n-\frac{1}{2}\mathrm{i}\Omega\right)^{(n)}(-1)^n}{(n+1)(n+1+a+b)n!},$$

$$a+b = 1+\frac{2\mathrm{i}\Omega}{\gamma+1}, \quad ab = \frac{\mathrm{i}\Omega(2+\mathrm{i}\Omega)}{2(\gamma+1)},$$

and $x^{(n)} = x(x+1)(x+2)\ldots(x+n-1)$ is the rising factorial. It is important to note that the second homogeneous solution behaves like $(1-\xi)^{-1-2\mathrm{i}\Omega/(\gamma+1)}$ as $\xi \to 1$. The terms a_0, b_0 and σ_r are unknowns. These can be found by applying appropriate boundary conditions. With this done, the solution to (2.24*b*) is found and the solutions to (2.24*a*) and (2.24*c*) follow.

2.3.2. *Linear analysis for a choked nozzle*

Consider a nozzle with geometry shown in figure 1. Apart from the uniform upstream and downstream regions of the duct, the nozzle is made up of three regions,

each with a linear steady velocity profile. The geometry is chosen such that the compactness of the contraction $|\Omega_c|$ is the same as that of the expansion downstream of the shock, and the compactness of the expansion upstream of the shock is chosen such that (2.10) holds true across the shock. It is assumed that the movement of the shock is small in comparison with the wavelengths of the disturbances at the shock, so that the boundary between the supersonic and subsonic regions in the expansion may be treated as stationary. Since linear theory predicts that the amplitude of the shock displacement is proportional to the amplitude of the excitation, there exists a sufficiently small excitation amplitude to satisfy this assumption. It is important to note that this may be a more strict limitation on the linearity of the system than the earlier assumption that second- and higher-order terms of the perturbation quantities are negligible.

First consider the contraction. Three boundary conditions are required to solve for the three unknowns a_0, b_0 and σ_r. The term ξ is unity at the throat, thus the singularity in P_{h2} can only be avoided by setting $b_0 = 0$. The downstream travelling pressure wave entering the system from the uniform upstream region is known. Let $p^+ = P^+ \exp(\mathrm{i}\omega t)$, $p^- = P^- \exp(\mathrm{i}\omega t)$ and the subscript $(\,)_u$ refer to quantities taken at the upstream entrance to the nozzle. Since σ_u is a known system excitation, if $x_r = x_u$ then $\sigma_r = \sigma_u$ is also known. Since P_u^+ is another known system excitation, then (2.3*a*) can be used to solve for the only remaining unknown a_0.

Next consider the expansion upstream of the shock. Again, since this region is bounded by the throat, it is necessary that $b_0 = 0$. The entropy wave and downstream travelling pressure wave are continuous across the throat. Since all the perturbations within the contraction have been found, σ at the throat is also known. Letting $x_r = x_*$, then $\sigma_r = \sigma_*$ can be used as a boundary condition. P^+ is also known at the throat, so (2.3*a*) can then be used to solve for the remaining unknown a_0. Note that it is not necessarily true that P^- is continuous across the throat. These final two boundary conditions are a result of solving the mass, momentum and energy conservation equations across the throat, as discussed in the Appendix.

Finally, consider the expansion downstream of the shock. The upstream travelling pressure wave entering the system from the uniform downstream region is known. Let the subscript $(\,)_d$ refer to quantities taken at the exit of the nozzle. Since P_d^- is known, then (2.3*b*) gives one boundary condition. With all the perturbations upstream of the shock solved, (2.20*a*) relates U_2 to P_2, giving a second boundary condition and (2.20*b*) relates σ_2 to P_2, giving the final boundary condition. Although the boundary conditions for the other regions of the nozzle allow each unknown to be found one at a time, the three boundary conditions for this final region of the nozzle must be solved simultaneously.

It is a relatively simple matter to extend this approach to nozzles with arbitrary geometries. The steady velocity distribution within the nozzle must first be approximated by a piecewise linear distribution. Each 'piece' of the steady velocity distribution can then be connected using a simple set of boundary conditions following a similar approach to that just discussed. Provided that the interface Mach number is not unity, the three boundary conditions used to connect each section are easily obtained by using the fact that P, U and σ are all continuous across each interface.

2.3.3. *Linear analysis for a supersonic diffuser*

This section describes the changes to the theory discussed in § 2.3.2 required to analyse a supersonic diffuser. Again, the geometry shown in figure 1 will be used. The flow in the contraction is supersonic, which has the result that p_u^- is travelling

	Response to P_u^+	Response to σ_u	Response to P_d^-
P_u^-	$\frac{2-[\gamma-1]\bar{M}_u}{2+[\gamma-1]\bar{M}_u}$	$\frac{-2\bar{M}_u}{2+[\gamma-1]\bar{M}_u}$	0
σ_d	$\frac{(\gamma-1)(1-\bar{M}_d)(2-[\gamma-1]\bar{M}_d)}{(1+[\gamma-1]\bar{M}_d)(2+[\gamma-1]\bar{M}_u)}$	$\frac{[\gamma-1]\bar{M}_d^2+\gamma[\gamma-1]\bar{M}_u\bar{M}_d+[\gamma-1]\bar{M}_d+2}{(1+[\gamma-1]\bar{M}_d)(2+[\gamma-1]\bar{M}_u)}$	$\frac{-(\gamma-1)(1-\bar{M}_d)}{1+[\gamma-1]\bar{M}_d}$
P_d^+	$\frac{2\bar{M}_d(3\gamma-1+\bar{M}_d^2[\gamma-1]^2)}{(1+\bar{M}_d)(1+[\gamma-1]\bar{M}_d)(2+[\gamma-1]\bar{M}_u)}$	$\frac{2\bar{M}_d(1-\gamma\bar{M}_u+[\gamma-1]\bar{M}_d^2)}{(1+\bar{M}_d)(1+[\gamma-1]\bar{M}_d)(2+[\gamma-1]\bar{M}_u)}$	$\frac{(1-\bar{M}_d)(1-[\gamma-1]\bar{M}_d)}{(1+\bar{M}_d)(1+[\gamma-1]\bar{M}_d)}$

TABLE 1. Reflection and transmission coefficients for a compact choked nozzle.

downstream. Therefore all three characteristics at the diffuser inlet are known system excitations. The resulting boundary conditions for the contraction are given by (2.3*a*,*b*), and $\sigma_r = \sigma_u$ with $x_r = x_u$. These boundary conditions give the three unknowns for the contraction region (a_0, b_0 and σ_r). It is no longer possible to choose $b_0 = 0$, so P_{h2} is singular at $\xi = 1$. Letting $(\,)_T$ designate quantities at the throat, the linear theory predicts that as $\bar{M}_T \to 1$, $P \to \infty$. Therefore, for sufficiently small values of $\bar{M}_T - 1$, the assumption of linearity will not hold. It follows that linear theory is insufficient to describe the frequency-dependent forced response of a supersonic diffuser for $\bar{M}_T - 1$ below some, yet to be determined, threshold value.

For sufficiently large values of $\bar{M}_T - 1$, it is a straightforward matter to model the remainder of the diffuser. P, U and σ at the throat are known from the analysis of the contraction, and since $\bar{M}_T \neq 1$, then they are continuous across the throat. This fact can be used to solve for a_0, b_0 and σ_r in the expansion upstream of the shock. The expansion downstream of the shock can be treated in exactly the same manner as for a choked outlet.

2.4. *Compact transmission and reflection coefficients for a choked nozzle*

It is often reasonable to assume that a nozzle is compact in comparison to the wavelengths of the acoustic and entropy waves in the system. The analytical results given in § 2.3.2 can be further simplified with the substitution $\Omega = 0$ to gain the compact reflection and transmission coefficients as given in table 1. The reflection coefficients agree with those of Marble & Candel (1977) and Stow, Dowling & Hynes (2002); however, the transmission coefficients appear to be a new contribution. Alternatively, these results may be derived directly from conservation across a compact nozzle. Therefore

$$M_u = \bar{M}_u, \qquad \frac{\rho_u u_u}{\bar{\rho}_u \bar{u}_u} = \frac{\rho_d u_d}{\bar{\rho}_d \bar{u}_d}, \qquad T_{t,u} = T_{t,d}, \tag{2.26a–c}$$

where the subscript $(\,)_t$ refers to stagnation quantities. The equations

$$\frac{p'}{\gamma \bar{p}} = \tfrac{1}{2}(p^+ + p^-), \quad \frac{u'}{\bar{c}} = \tfrac{1}{2}(p^+ - p^-), \quad \frac{\rho'}{\bar{\rho}} = \frac{p'}{\gamma \bar{p}} - \frac{s'}{c_p} \tag{2.27a–c}$$

can then be substituted into (2.26*a*)–(2.26*c*), giving three equations in the three unknown outgoing waves (p_u^-, p_d^+ and s_d'/c_p). These equations can be linearized in the wave amplitudes and solved to gain the same compact reflection and transmission coefficients as given in table 1. Alternatively, the equations may be left in the nonlinear form and solved numerically in order to obtain the nonlinear behaviour of a compact choked nozzle.

	Response to P_u^+	Response to σ_u	Response to P_u^-
σ_d	$\frac{(\gamma-1)(1+\bar{M}_u)(\bar{M}_u\mathscr{M}_d-\bar{M}_d\mathscr{M}_u)}{2\bar{M}_u\mathscr{M}_u(1+[\gamma-1]\bar{M}_d)}$	$\frac{\mathscr{M}_d+[\gamma-1]\bar{M}_d\mathscr{M}_u}{\mathscr{M}_u(1+[\gamma-1]\bar{M}_d)}$	$\frac{(\gamma-1)(1-\bar{M}_u)(\bar{M}_u\mathscr{M}_d+\bar{M}_d\mathscr{M}_u)}{2\bar{M}_u\mathscr{M}_u(1+[\gamma-1]\bar{M}_d)}$
P_d^+	$\frac{\bar{M}_d(1+\bar{M}_u)(\mathscr{M}_u+[\gamma-1]\bar{M}_u\mathscr{M}_d)}{\bar{M}_u\mathscr{M}_u(1+\bar{M}_d)(1+[\gamma-1]\bar{M}_d)}$	$\frac{2(\gamma-1)\bar{M}_d(\bar{M}_d^2-\bar{M}_u^2)}{\mathscr{M}_u(1+\bar{M}_d)(1+[\gamma-1]\bar{M}_d)}$	$\frac{\bar{M}_d(\bar{M}_u-1)(\mathscr{M}_u-[\gamma-1]\bar{M}_u\mathscr{M}_d)}{\bar{M}_u\mathscr{M}_u(1+\bar{M}_d)(1+[\gamma-1]\bar{M}_d)}$

TABLE 2. Reflection and transmission coefficients for a compact supersonic diffuser, where $\mathscr{M} = 2 + (\gamma - 1)\bar{M}^2$. The response to P_d^- is not shown as it is the same as for a compact choked nozzle.

2.5. *Compact transmission and reflection coefficients for a supersonic diffuser*

Despite the difficulties faced in § 2.3.3, it is possible to formulate reflection and transmission coefficients for a compact supersonic diffuser regardless of the value of $\bar{M}_T$. The equations governing a compact supersonic diffuser are very similar to those for a compact choked nozzle. Equations (2.26*b*) and (2.26*c*) are still true, although now (2.26*a*) is no longer true. Substituting the characteristic definitions into (2.26*b*) and (2.26*c*) will yield two equations in the two unknown outgoing waves (p_d^+ and s_d'/c_p). Linearizing these equations in the wave amplitudes will give the reflection and transmission coefficients as shown in table 2. These coefficients do not appear to have been previously presented. Again, the linearization may be skipped and numerical solution of the equations will predict the nonlinear system behaviour.

2.6. *Unchoke criterion for a choked nozzle*

As discussed in § 2.2, disturbances interact with a normal shock wave and cause it to move. If these disturbances are large enough to cause the shock to travel to a position upstream of the nozzle throat, then the nozzle will no longer be choked, and a large deviation from the behaviour predicted by the present theory is expected. As such, it is useful to be able to give conditions for 'unchoke'.

Unchoke cannot be predicted using the linear theory presented in § 2.3.2. If the amplitude of x_s' is greater than the distance between the steady shock location and the throat, then unchoke is experienced. However, the discussion in § 2.3.2 assumes that x_s' is small in comparison to the wavelength of the disturbances at the shock. The speed at which p^- travels is $\bar{c}(1-\bar{M})$, so p^- is stationary at the throat, and the wavelength of p^- is zero, contradicting the initial assumption. Therefore an alternative analysis must be applied. Development of a frequency-dependent unchoke criterion is a difficult task since, for high-frequency excitation, multiple shocks may exist within the nozzle, as discussed later. The theory discussed in this paper will therefore only be concerned with an unchoke criterion for compact nozzles.

Consider the instant at which the shock momentarily reaches the nozzle. Equations (2.26*a*)–(2.26*c*) still hold at this instant. The shock becomes infinitely weak as it reaches the throat, so the flow between the nozzle inlet and nozzle outlet is isentropic. This can be represented by an isentropic relation between the inlet and outlet, such as $p_{t,u} = p_{t,d}$. This gives a total of four equations. However, at this stage of the analysis, the amplitudes of all six waves at the nozzle boundaries are unknown. The final two equations must be gained from assuming something about the excitation. For example, it might be assumed that two of the three excitation waves are known. A simple numerical solver could then be used to find the amplitude of the remaining excitation wave required to cause unchoke (alternatively the equations

may be linearized and solved algebraically; however, since unchoke often requires large excitation amplitudes, the application of a linear analysis will be limited). Using an approach like this, the critical value of p_d^- could be found for a range of combinations of p_u^+ and s_u'/c_p in order to completely map the boundary between choke and unchoke regimes in $(p_u^+, s_u'/c_p, p_d^-)$ space.

2.7. *'Over-choke' criterion for a choked nozzle*

System excitation may alternatively cause the shock to travel through the outlet of the nozzle, which will be called 'over-choke'. The magnitude of excitation required to cause over-choke can be found using a similar technique to that given in § 2.6. Again, it is assumed that the nozzle is compact. Consider the moment just before over-choke, when the shock is just about to cross the junction between the expansion and the uniform downstream section. As with the calculations in § 2.6, (2.26*a*)–(2.26*c*) are still true and one further equation is required. This final equation is simply $M_d = M_2$. In order to express M_2 in terms of the wave amplitudes at the nozzle inlet and outlet, it is first necessary to employ the area–Mach number relation in order to obtain

$$\frac{g(\bar{M}_u)}{g(M_u)} = \frac{g(\bar{M}_1)g(\bar{M}_d)}{g(M_1)g(\bar{M}_2)}, \tag{2.28}$$

where

$$g(M) = M^2/\left[1 + \tfrac{1}{2}(\gamma - 1)M^2\right]^{(\gamma+1)/(\gamma-1)}.$$

This allows M_1 to be expressed in terms of the wave amplitudes at the inlet and outlet. The shock relation,

$$M_2^2 = \frac{1 + \frac{1}{2}(\gamma - 1)M_1^2}{\gamma M_1^2 - \frac{1}{2}(\gamma - 1)}, \tag{2.29}$$

can then be used to express M_2 in terms of M_1.

2.8. *Unstart criteria for a compact supersonic diffuser*

The interaction of disturbances with a supersonic diffuser may result in the expulsion of a shock wave from the diffuser inlet. This process is referred to as 'unstart'. The unstart criteria for a compact supersonic diffuser can be developed following similar arguments to those given in § 2.6. In contrast to the choked nozzle, p_u^- is a system excitation rather than an unknown, so the number of equations required is reduced from four to three. Equations (2.26*b*) and (2.26*c*) still apply, so one equation remains to be found.

Two different mechanisms of unstart exist in a supersonic diffuser. In the first type of unstart, excitation causes the primary shock to travel upstream of the throat. When the shock reaches the throat $M_T = M_1$, giving the final required equation. In order to express M_T and M_1 in terms of the unknowns at the system boundaries, the area–Mach number relation can be used to show that

$$\frac{g(M_T)}{g(\bar{M}_T)} = \frac{g(M_u)}{g(\bar{M}_u)}, \tag{2.30a}$$

$$\frac{g(M_1)g(\bar{M}_2)}{g(\bar{M}_1)g(M_2)} = \frac{g(M_u)g(\bar{M}_d)}{g(\bar{M}_u)g(M_d)}. \tag{2.30b}$$

The second type of unstart occurs when the unsteady Mach number at the throat drops below unity. This results in the formation of a shock at the throat which, in the low frequency limit, is unstable and is expelled out of the nozzle inlet. The criterion

for this second type of unstart is $M_T = 1$, as shown by Mayer & Paynter (1995). Equation (2.30a) can again be used to express M_T in terms of p_u^+, p_u^- and σ_u to give a general condition for this second type of unstart. This also gives a physical explanation for the failure of the linear theory to describe a supersonic diffuser in the limit $\bar{M}_T \to 1$ as discussed in § 2.3.3. In such a case, an unstable shock will develop at the throat of the diffuser for infinitesimal forcing amplitudes. As $\bar{M}_T$ is increased from unity, it follows that the amplitude of forcing required to cause the second type of unstart will also increase.

2.9. *'Over-choke' criterion for a compact supersonic diffuser*

The 'over-choke' criterion for a compact supersonic diffuser can be developed following the arguments in § 2.7, except (2.26a) is no longer true and p_u^- is a system excitation rather than an unknown. Since the number of equations and unknowns have been reduced from four to three, a numerical solution for the 'over-choke' criterion can still be found.

3. Numerical solver

In this section, (2.1a)–(2.1c) are solved numerically in conservation form to validate the present theory and to study the effect of nonlinearity on the forced response of choked nozzles and supersonic diffusers. A dispersion-relation-preserving (DRP) scheme of Tam & Webb (1993) is adopted to perform the time marching and spatial differencing. The specific DRP scheme chosen uses an optimized fourth-order spatial and temporal discretization. The choice of such a scheme ensures that the computed waves are a good approximation of the exact solutions of the Euler equations.

Non-reflecting boundary conditions are implemented to ensure that the numerical domain approximates an infinite domain. The boundary conditions follow the formulation of Poinsot & Lele (1992) to ensure that the incoming waves at each boundary are equal to the desired values of the system excitation. This means that one of the incoming waves is sinusoidal with a fixed amplitude, and the rest are set to zero. The non-reflecting boundaries are placed very close to the nozzle inlet and outlet in order to reduce the effects of nonlinear wave propagation between the boundary of the numerical domain and the nozzle.

Limitations of the spatial differencing scheme, which uses a seven-point stencil, would produce very large non-physical numerical waves at a shock. These numerical waves can pollute the solution with unacceptable noise, so it is necessary to adopt a damping scheme. The adaptive nonlinear artificial dissipation model of Kim & Lee (2001) is used as they show it to perform very well for acoustic calculations within choked nozzles. After some testing, it was found that the simulations produce results with less noise if the adaptive control constant of Kim & Lee (2001) is set to a static value of 5 for the choked nozzle simulations and 10 for the supersonic diffuser simulations.

All simulations are run with a Courant–Friedrichs–Lewy number of 0.2. The number of gridpoints used in each simulation is 501. Simulations are run without excitation to a converged steady-state solution before harmonic excitation is started. Convergence to the steady state is assumed to be reached when the relative change in density between time steps is of a similar magnitude to the floating-point error. When convergence is reached, harmonic excitation is started, and the simulation is run for a sufficiently long time to ensure that the response is periodic.

A number of tests were performed to validate the numerical solver. These included linear acoustic and entropy propagation, the shock tube problem for shock dynamics

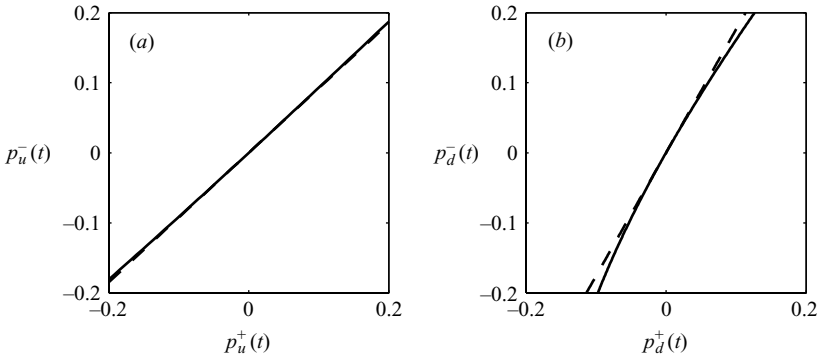

FIGURE 2. Pressure reflection behaviour of a compact nozzle, showing (*a*) p_u^- versus p_u^+ and (*b*) p_d^- versus p_d^+. Dashed lines show predicted linear response and solid lines show predicted nonlinear response. $\bar{M}_u = \bar{M}_d = 0.2$.

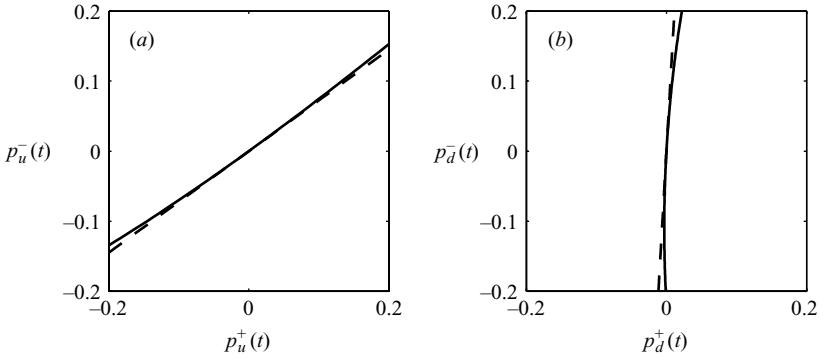

FIGURE 3. As for figure 2 except with $\bar{M}_u = \bar{M}_d = 0.8$.

and nonlinear wave propagation, and tests to ensure that the non-reflecting boundaries were behaving correctly. The good agreement between the present theory and the numerical results shown in § 4 is, in itself, validation of the numerical code.

4. Discussion

In this section, numerical simulations are performed on the geometries given in figure 1 for different forms of excitation waves and, where possible, the results are compared to the theory discussed in § 2.

4.1. *Compact behaviour*

Figure 2 shows the predicted nonlinear pressure reflection behaviour of a compact choked nozzle with $\bar{M}_u = \bar{M}_d = 0.2$. The linear results are, of course, straight lines with slopes equal to the pressure reflection coefficient P^-/P^+. As shown in figure 2(*a*), when the nozzle is behaving as an outlet (i.e. excitation coming from upstream) there is a very small difference between the linear and nonlinear results for amplitudes of excitation as high as $P_u^+ = 0.2$. Figure 2(*b*) suggests that there is a larger degree of nonlinearity in the pressure reflection behaviour when the nozzle is acting as an inlet (i.e. excitation coming from downstream).

Figure 3 suggests that the pressure reflection behaviour of the nozzle is more nonlinear when $\bar{M}_u = \bar{M}_d$ is increased. Define the ratio $|(R_{nl} - R_l)/R_{nl}|$, where R_{nl} is the instantaneous magnitude of the reflected acoustic wave given by the nonlinear

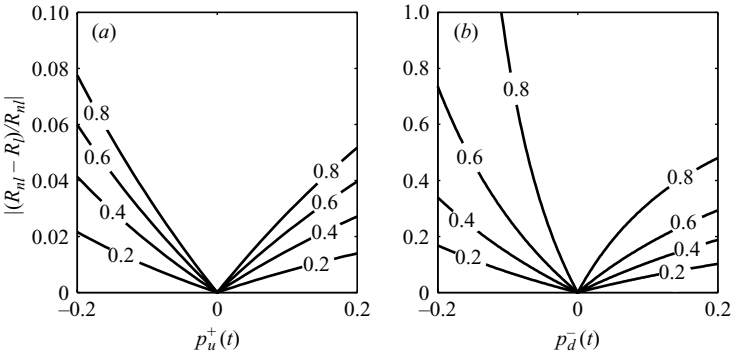

FIGURE 4. $|(R_{nl} - R_l)/R_{nl}|$ versus instantaneous forcing magnitude for compact choked nozzle acting as (*a*) an inlet and (*b*) an outlet. Contours show value of $\bar{M}_u = \bar{M}_d$.

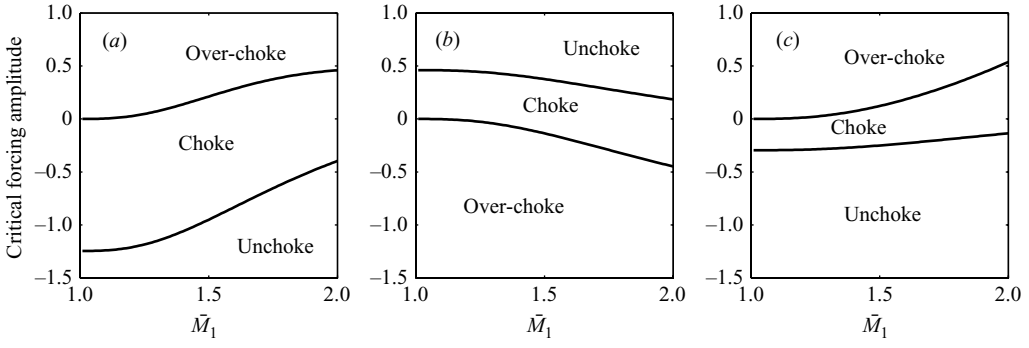

FIGURE 5. Critical forcing amplitudes required to cause unchoke and over-choke in a compact choked nozzle for forcing exclusively in (*a*) s_u'/c_p, (*b*) p_u^+, and (*c*) p_d^-. $\bar{M}_u = \bar{M}_d = 0.5$.

theory and R_l is the instantaneous magnitude of the reflected acoustic wave given by the linear theory. Figure 4 more clearly illustrates the effect of Mach number on the nonlinearity of the acoustic reflection behaviour. Some insight into this trend can be gained by considering the limit as $\bar{M}_u, \bar{M}_d \to 0$. At this limit, the area of the throat approaches zero, so the nozzle is closed. In one-dimensional acoustics, a closed end has perfectly linear reflection ($p^+ = p^-$), suggesting increasing nonlinearity at higher Mach numbers.

Figure 5 shows the amplitude of forcing required to cause unchoke and over-choke in a compact choked nozzle for forcing in s_u'/c_p, p_u^+ and p_d^-. Placing the shock towards the upstream end of the nozzle (decreasing $\bar{M}_1$) increases the forcing amplitude required to cause over-choke but decreases the forcing amplitude required to cause unchoke, which is unsurprising. The trends in critical forcing amplitudes for supersonic diffusers are very similar, although a second mechanism of unchoke may occur (see § 2.8), significantly reducing the critical forcing amplitudes for throat Mach numbers close to unity.

Figure 6 shows a time trace of the reflected pressure wave from a compact choked nozzle acting as an inlet. For this configuration, the amplitude of forcing in p_d^- required to cause unchoke is 0.0915. The figure shows that when the amplitude of forcing is below 0.0915, the nonlinear analysis agrees well with the Euler simulation at low frequency. The small phase difference between the simulation and the nonlinear

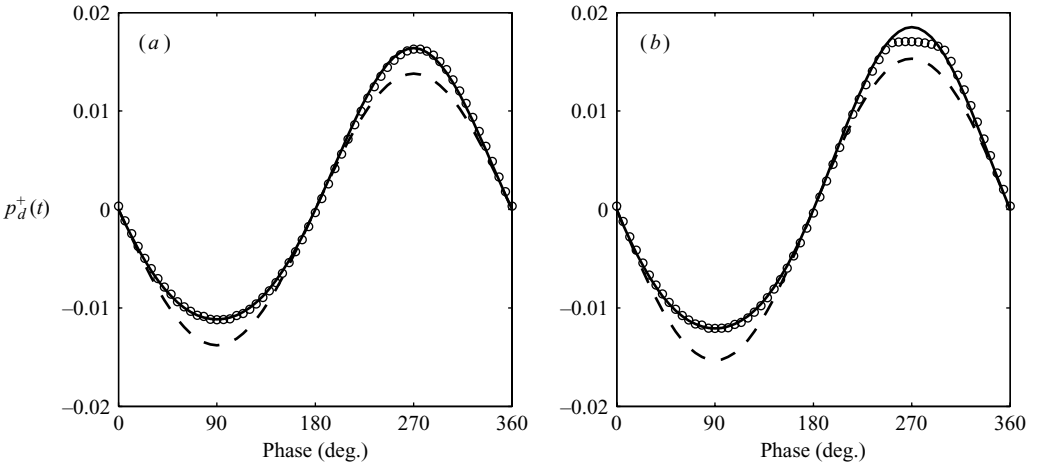

FIGURE 6. Time trace of reflected pressure from a compact choked nozzle with harmonic forcing of p_d^- with (*a*) $P_d^- = 0.09$ and (*b*) $P_d^- = 0.1$. $|\Omega_c| = 0.01$, $\bar{M}_u = \bar{M}_d = 0.6$ and $\bar{M}_1 = 1.4$. Nonlinear prediction (solid line); linear prediction (dashed line); simulation (○).

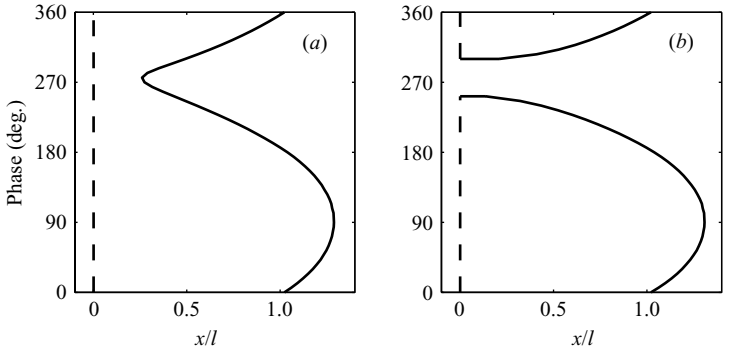

FIGURE 7. Simulated shock location in a compact choked nozzle with harmonic forcing in p_d^- with (*a*) $P_d^- = 0.09$ and (*b*) $P_d^- = 0.1$. $|\Omega_c| = 0.01$, $\bar{M}_u = \bar{M}_d = 0.6$ and $\bar{M}_1 = 1.4$. Shock location (solid line); unsteady sonic point (dashed line). l is the length of the contraction. Throat located at $x/l = 0$.

analytical result is due to the fact that the simulation results are for $|\Omega_c| = 0.01$ (running the simulation at $\Omega_c = 0$ would require an infinite amount of time). Unchoke occurs when the amplitude of forcing is increased above 0.0915, and there is worse agreement with the nonlinear analytical result only while the nozzle is unchoked. This is supported by figure 7, which shows the time-dependent location of the shock and the sonic point. It is also interesting to note that the non-sinusoidal motion of the shock wave shown in figure 7(*a*) nonetheless results in a comparatively sinusoidal reflected wave.

4.2. *Frequency-dependent behaviour of choked nozzles*

Culick & Rogers' (1983) study of the shock dynamics in a supersonic diffuser neglected the effect of the contraction and expansion on the acoustics, but conceded that it may be important. Figure 8 investigates this effect, showing the linear theory for the reflection coefficient P_d^+/P_d^- for a nozzle. Also shown is the predicted reflection coefficient of the shock, neglecting the effect of the change in geometry on the

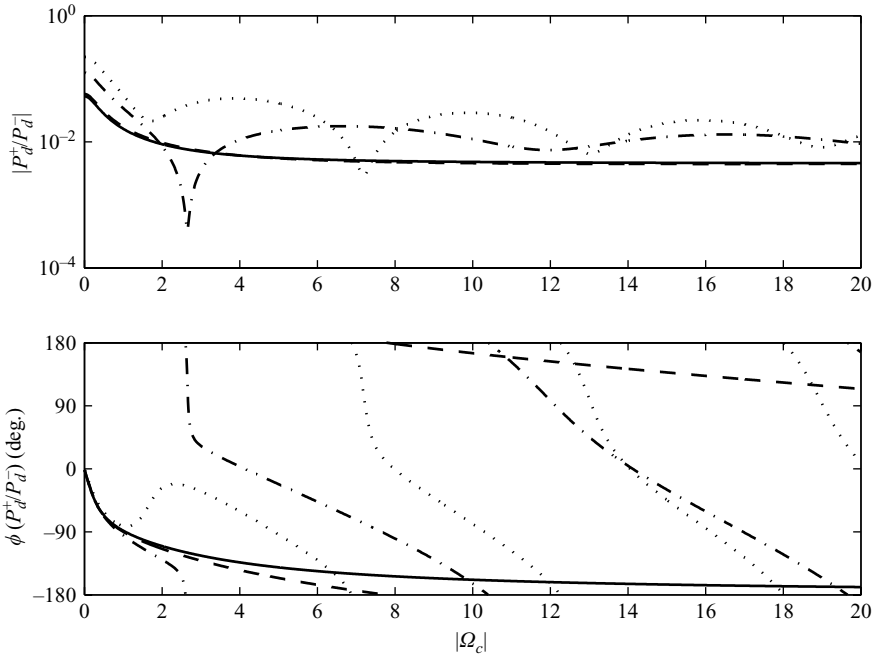

FIGURE 8. Pressure reflection coefficient P_d^+/P_d^- versus compactness $|\Omega_c|$ from linear theory. $\bar{M}_u = 0.5$ and $\bar{M}_1 = 1.25$. Shock only (solid line); $\bar{M}_d = 0.8$ (dashed line); $\bar{M}_d = 0.65$ (dash-dotted line); $\bar{M}_d = 0.5$ (dotted line).

acoustics. The difference between the two results is dependent on the difference between $\bar{M}_d$ and $\bar{M}_2$. If they are similar, then the area change between the shock and the nozzle exit is small, so the effect of the area change is also small. This is evident in the $\bar{M}_d = 0.8$ curve since $\bar{M}_2 \approx 0.81$. Conversely, when $\bar{M}_d$ is quite different to $\bar{M}_2$, the effect of the area change is large, as is shown by the $\bar{M}_d = 0.5$ curve.

All numerical simulations involve sinusoidal excitation in one of the incoming characteristic waves. If the system exhibits perfectly linear behaviour, then the outgoing waves will have the same spectral content as the excitation. Since the Euler equations are nonlinear, it is necessary to develop an appropriate method for determining the phase and magnitude of some general nonlinear response. Let the series f denote the outgoing characteristic being analysed over a full forcing period. The discrete Fourier transform and the inverse discrete Fourier transform can then be used to isolate f_ω, defined as the component of f occurring at the excitation frequency. The phase and magnitude of f_ω can then be used as measures of the phase and magnitude of f. The difference between f and f_ω can also be used as a measure of nonlinearity, defined as

$$\mu = \frac{|f - f_\omega|_2}{|f|_2}, \tag{4.1}$$

where $|\,|_2$ denotes the ℓ^2-norm. When $\mu = 0$, the response is sinusoidal at the input frequency, i.e. an exactly linear response. Conversely, when $\mu = 1$, the response has no spectral content at the forcing frequency, i.e. it is strongly nonlinear. As such, determination of the phase and magnitude of f_ω is only meaningful for systems with values of μ close to zero.

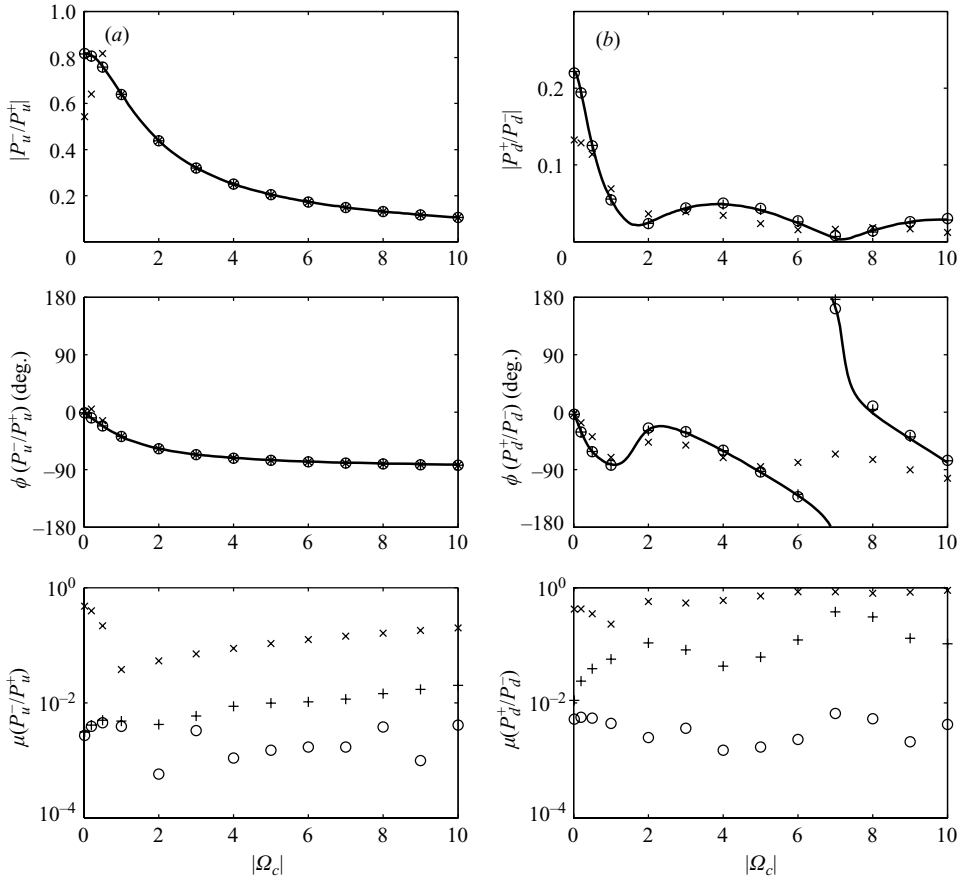

FIGURE 9. Frequency-dependent pressure reflection coefficient for choked nozzle with $\bar{M}_u = \bar{M}_d = 0.5$ and $\bar{M}_1 = 1.25$, (*a*) outlet and (*b*) inlet. Linear theory (solid line), and simulation results for forcing amplitudes of 10^{-5} (○), 10^{-2} (+) and 10^{-1} (×).

Figure 9 shows the frequency dependence of the reflection coefficient when the nozzle is acting as an inlet and as an outlet. As the frequency of forcing increases, the magnitudes of the reflection coefficients decrease for both configurations. Although Marble & Candel (1977) do not consider the effect of the shock, no information from the shock is able to be transmitted upstream through the supersonic region downstream of the throat. It therefore follows that their results for the choked outlet reflection coefficient agree with those presented here since they are unaffected by the shock. The magnitude of the inlet pressure reflection coefficient exhibits a number of local maxima. The period associated with the frequency gap between each of these maxima is roughly equal to the transport lag of an acoustic wave travelling from the uniform downstream section to the shock and back again.

The agreement between the analytical and simulated reflection coefficients in figure 9 is very good up to forcing amplitudes of 10^{-2}. At a forcing amplitude of 10^{-5}, the nonlinearity measure for both the inlet and outlet is less than 0.01 across all frequencies tested. This validates the linear theory and the numerical scheme. At this forcing amplitude, the magnitude of the shock displacement is smaller than the grid spacing. For larger excitation amplitudes, the shock may pass through gridpoints, causing

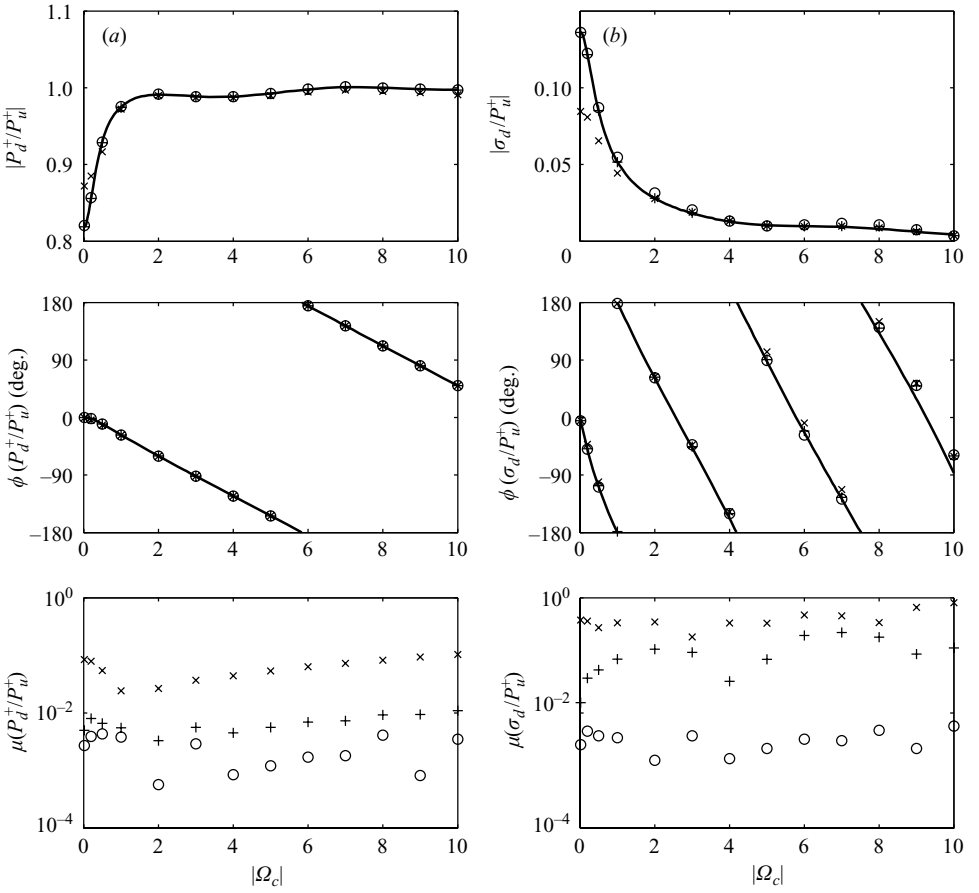

FIGURE 10. Frequency-dependent transmission coefficient for choked nozzle with $\bar{M}_d = \bar{M}_u = 0.5$ and $\bar{M}_1 = 1.25$. (*a*) P_d^+/P_u^+ (*b*) and σ_d/P_u^+ . Theory (solid line), and simulation results for forcing amplitudes of 10^{-5} (○), 10^{-2} (+) and 10^{-1} (×).

numerical noise to enter the solution downstream of the shock. When observing waves of comparable amplitudes to the excitation wave, this noise has a negligible effect; however, it can have a more significant effect on waves of smaller amplitudes. This manifests as an over-prediction of μ for some of the numerical results presented. In particular, when the forcing amplitude is 10^{-2} and 10^{-1} and $|\Omega_c| > 1$, there is an over-prediction of $\mu(P_d^+/P_d^-)$.

For all frequencies and forcing amplitudes tested, the outlet is more linear than the inlet, which is in agreement with the predictions for compact nozzles discussed in § 2.4. The behaviour of the outlet is considerably more nonlinear when $|\Omega_c| < 1$ and the forcing amplitude is 10^{-1} than it is at the other operating conditions tested. This is due to periodic unchoking of the nozzle under these conditions.

Figure 10 shows the frequency dependence of the transmission coefficients P_d^+/P_u^+ and σ_d/P_u^+ for a choked nozzle. Again, the phase and amplitude of the numerical results agrees well with the linear theory up to a forcing amplitude of 10^{-2}. At a forcing amplitude of 10^{-5}, the nonlinearity is less than 0.01. The phase of P_d^+/P_u^+ is approximately equal to the transport lag of a pressure wave travelling from the nozzle inlet to the nozzle outlet. P_d^+/P_u^+ only shows substantial nonlinearity at a forcing

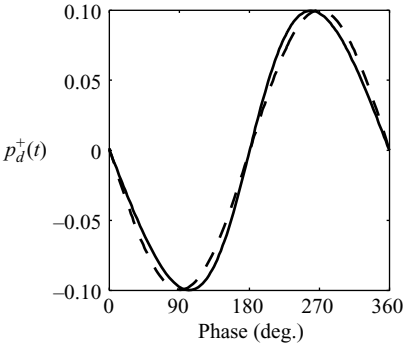

FIGURE 11. Time trace of transmitted acoustic wave with forcing in p_u^+. $P_u^+ = 10^{-1}$, $|\Omega_c| = 10$, $\bar{M}_u = \bar{M}_d = 0.5$ and $\bar{M}_1 = 1.25$. Simulated result (solid line); linear prediction (dashed line).

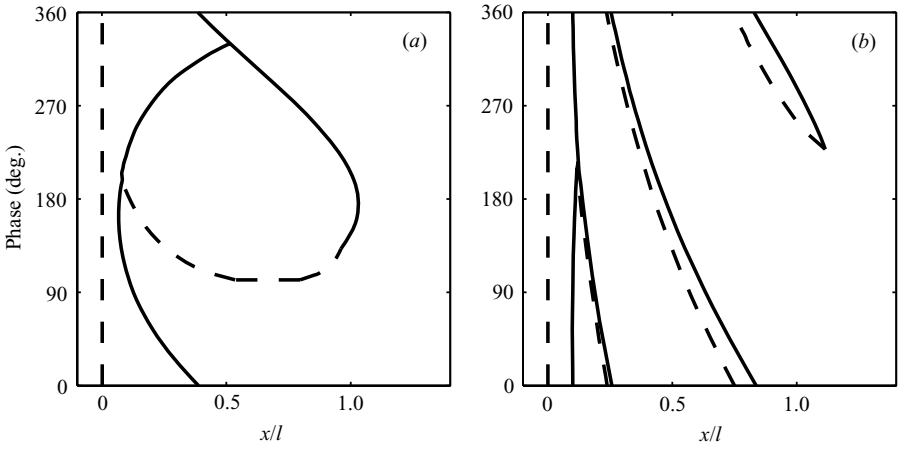

FIGURE 12. Simulated shock location in a choked nozzle with harmonic forcing in p_d^-. (*a*) $P_d^- = 0.167$ and $|\Omega_c| = 1$ and (*b*) $P_d^- = 0.307$ and $|\Omega_c| = 5$. $\bar{M}_u = \bar{M}_d = 0.5$ and $\bar{M}_1 = 1.4$. Shock location (solid line); unsteady sonic point (dashed line). l is the length of the contraction. Throat located at $x/l = 0$.

amplitude of 10^{-1}, where for $|\Omega_c| < 1$, the nozzle unchokes, and for higher frequencies, wave steepening has an increasing effect. A typical transmitted wave showing effects of wave steepening is shown in figure 11. For forcing of sufficiently large amplitude and/or frequency, wave steepening may even result in the development of sawtooth waves containing shocks.

The shock motion can also be significantly different at higher frequencies than it is in the $\omega \to 0$ limit. As shown in figure 12(*a*), during the motion of the shock upstream, the flow further downstream of the shock accelerates until it becomes supersonic and a new shock is eventually formed. The acceleration of the flow behind the original shock causes it to reduce in strength until it starts travelling upstream. The weak original shock eventually coalesces with the stronger new shock, having little effect on its motion. After a full period of excitation, the new shock ends up at the same location as the original shock. Increasing the excitation frequency further allows for the existence of even more shocks within the nozzle (figure 12*b* shows three shocks when $|\Omega_c| = 5$). This agrees with the results of Rein, Grabitz & Meier (1988), who studied shock motion using a different numerical method.

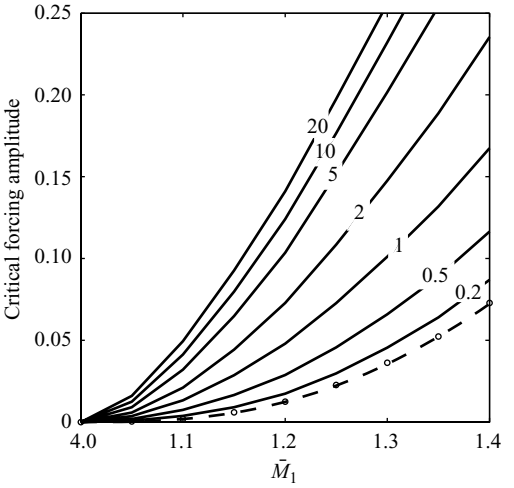

FIGURE 13. P_d^- required to cause unchoke in a choked nozzle with $\bar{M}_u = \bar{M}_d = 0.5$. Solid lines show simulation results. Contour labels give value of $|\Omega_c|$. Dashed line shows theoretical result for compact choked nozzle. Circles show simulated results for $|\Omega_c| = 0.01$.

The frequency dependence of the forcing amplitude required to cause unchoke is shown in figure 13 for the case of harmonic excitation in p_d^-. The agreement between the theory for a compact choked nozzle and the simulations for $|\Omega_c| = 0.01$ is very good. As the forcing frequency increases, a greater forcing amplitude is required to cause unchoke. As discussed in § 2.6, developing a general formula for this frequency dependence would be a very difficult task.

4.3. *Frequency-dependent behaviour of supersonic diffusers*

The pressure transmission behaviour of a supersonic diffuser with $\bar{M}_T = 1.01$ is shown in figure 14. The linear theory and numerical results for forcing amplitudes of 10^{-5} agree well. This shows that the linear theory is still valid for the range of throat Mach numbers typical in most practical engineering applications despite its limitations as $\bar{M}_T \to 1$ (see § 2.3.3). Although not shown, further reduction of the throat Mach number results in a more appreciable deviation from the linear theory until $\bar{M}_T = 1$, when the linear theory becomes singular.

When the forcing amplitude is increased at low frequencies, the supersonic diffuser experiences the second type of unstart as described in § 2.8. Because the motion of the shock past the inlet causes an abrupt change in the inlet conditions, it is non-physical to make observations on the transmission coefficient. The results affected by this second type of unstart are therefore omitted from figure 14. When this second form of unstart does not occur, the simulation results for a forcing amplitude of 10^{-2} have a nonlinearity measure of less than 0.01, suggesting a strongly linear behaviour. At a forcing amplitude of 10^{-1} a small amount of nonlinearity due to wave steepening is observable.

The second type of unstart is illustrated in figure 15(*a*), which shows formation of a shock just upstream of the throat. Since the example shown is for a finite-length supersonic diffuser, the new shock takes some time to travel all the way upstream to the nozzle inlet. In the case of a compact supersonic diffuser, the shock instantly reaches the nozzle inlet. Increasing the frequency further (as shown

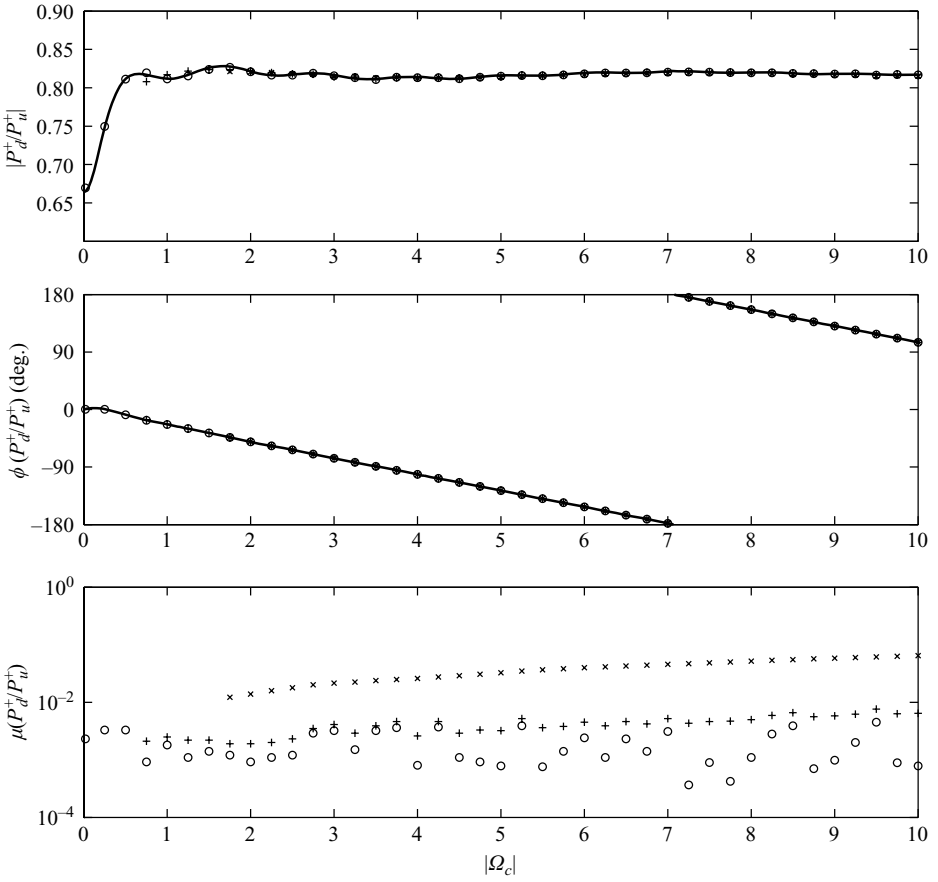

FIGURE 14. Frequency-dependent pressure transmission coefficient for a supersonic diffuser with $\bar{M}_u = 1.5$, $\bar{M}_d = 0.5$, $\bar{M}_1 = 1.25$, and $\bar{M}_T = 1.01$. Theory (solid line), and simulation results for forcing amplitudes of 10^{-5} ($\circ$), 10^{-2} ($+$) and 10^{-1} ($\times$).

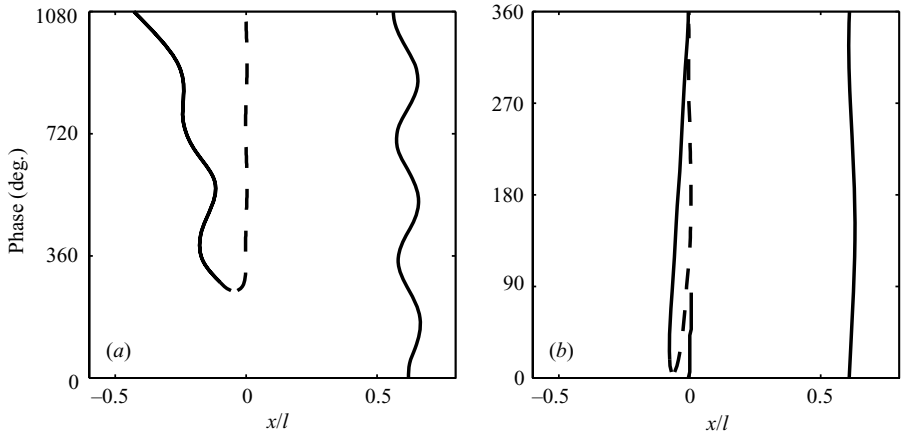

FIGURE 15. Simulated shock location in a supersonic diffuser with harmonic forcing of $P_u^+ = 0.0167$, (*a*) $|\Omega_c| = 0.5$ and (*b*) $|\Omega_c| = 1.75$. $\bar{M}_u = 1.5$, $\bar{M}_d = 0.5$ and $\bar{M}_1 = 1.25$. Shock location (solid line); unsteady sonic point (dashed line). l is the length of the contraction. Throat located at $x/l = 0$.

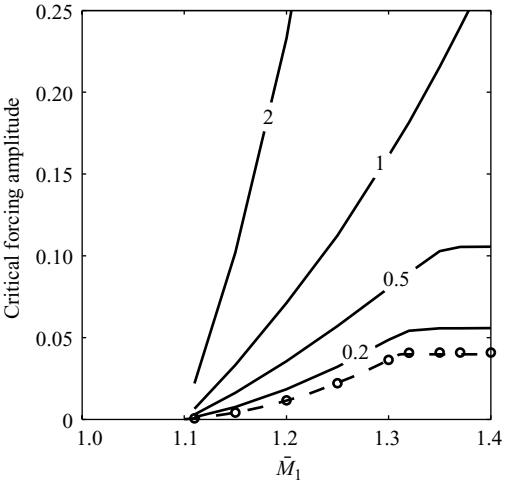

FIGURE 16. P_u^+ required to cause unstart in a supersonic diffuser with $\bar{M}_u = 1.5$, $\bar{M}_T = 1.1$ and $\bar{M}_d = 0.5$. Solid lines show simulation results. Contour labels give value of $|\Omega_c|$. Dashed line shows theoretical result for compact supersonic diffuser. Circles show simulated results for $|\Omega_c| = 0.01$.

in figure 15*b*), the shock may never reach the nozzle inlet, instead travelling back towards the throat where it disappears shortly after the formation of a new stable shock.

Figure 16 shows the frequency dependence of the forcing amplitude required to cause unstart for the case of harmonic excitation in p_u^+. The compact theory predicts that for $\bar{M}_1 = \bar{M}_T$, the primary shock will travel past the throat (resulting in unstart) for infinitesimally small harmonic forcing. As $\bar{M}_1$ is increased from $\bar{M}_T$, the amplitude required to cause the primary shock to travel past the throat steadily increases. At a sufficiently large value of $\bar{M}_1$, it is not possible to cause the primary shock to travel past the throat. Instead the excitation results in the reduction of the throat Mach number to unity, at which point the second mechanism of unstart occurs instead. The amplitude of forcing required to cause the second mechanism of unstart is independent of $\bar{M}_1$, so a levelling of the critical forcing amplitude is observed at higher $\bar{M}_1$. Figure 16 shows that the nonlinear compact theory agrees well with simulations performed at $|\Omega_c| = 0.01$. As also observed with unchoke of choked nozzles, the amplitude of forcing required to cause unstart increases with frequency.

5. Conclusions

A linear analytic model for studying the frequency response of arbitrarily shaped nozzles was developed. This was validated for the case of simple choked nozzle and supersonic diffuser geometries using numerical simulations of the quasi-one-dimensional Euler equations. This model adds to existing works since it includes the effects of geometry, forcing frequency and the existence of a normal shock within the expansion. All of these have been shown to have a strong effect on the nozzle and diffuser response in certain circumstances.

All of the compact transmission and reflection coefficients for choked nozzles and supersonic diffusers have also been identified and evaluated. It appears that this is the first time that several of the compact transmission coefficients have been presented.

The response of choked nozzles and supersonic diffusers to larger amplitude excitation was then investigated numerically and analytically. A range of different nonlinear effects were identified. It was shown that the equations governing the response of a compact choked outlet were more linear than those governing the behaviour of a compact choked inlet. It was also shown that higher Mach numbers upstream and downstream of choked nozzles contribute to a more nonlinear response. Wave steepening had a noticeable effect only for forcing with sufficiently large amplitude and/or frequency. Typically, the most significant nonlinear effects were unchoke, unstart and 'over-choke'. If these were avoided by appropriate placement of the shock, the forced response of the nozzle/diffuser was strongly linear for forcing amplitudes up to $P_u^+ = 0.01$. Nonetheless, nonlinearity in nozzle and diffuser response appears to be significant at forcing amplitudes typically experienced in some engineering devices.

Since unchoke, unstart and 'over-choke' were found to have a strong nonlinear effect, an analytical model for their prediction was developed and validated against numerical simulations. Unsurprisingly, it was found that unchoke and the first mechanism of unstart occurred more readily if the shock was located close to the throat, and 'over-choke' occurred more readily if the shock was located close to the nozzle exit. The second mechanism of unstart was shown to occur more readily if the throat Mach number was close to unity. Of more significance, the numerical results also showed that by increasing the forcing frequency, a progressively larger forcing amplitude was required to cause unchoke, unstart or 'over-choke' because shock motion decreases with increasing forcing frequency.

Appendix. Solution of conservation equations across the throat

Consider solving (2.1*a*)–(2.1*c*) across an infinitesimally wide section through the throat. Since the section at the throat is of infinitesimal width, then it has no storage capacity and any time derivatives in the conservation equations can be dropped. Linearizing in the perturbation quantities gives

$$p^+_{u*} - \frac{s_{u*}{}'}{c_p} = p^+_{d*} - \frac{s_{d*}{}'}{c_p}, \tag{A 1a}$$

$$2p^+_{u*} - \frac{s_{u*}{}'}{c_p} = 2p^+_{u*} - \frac{s_{d*}{}'}{c_p}, \tag{A 1b}$$

$$\frac{3\gamma - 1}{2\gamma - 2} p^+_{u*} - \frac{s_{u*}{}'}{c_p} = \frac{3\gamma - 1}{2\gamma - 2} p^+_{d*} - \frac{s_{d*}{}'}{c_p}, \tag{A 1c}$$

where $(\,)_{u*}$ denotes quantities taken at the upstream side of the throat and $(\,)_{d*}$ denotes quantities taken at the downstream side of the throat. One of these equations is redundant, and all three can be satisfied iff $p^+_{u*} = p^+_{d*}$ and $s_{u*}{}' = s_{d*}{}'$. It is not necessary for $p^-_{u*} = p^-_{d*}$.

REFERENCES

Culick, F. E. C. & Rogers, T. 1983 The response of normal shocks in diffusers. *AIAA J.* **21**, 1382–1390.

Dowling, A. P. & Hubbard, S. 2000 Instability in lean premixed combustors. *Proc. Inst. Mech. Engrs* A **214**, 317–332.

Kim, J. W. & Lee, D. J. 2001 Adaptive nonlinear artificial dissipation model for computational aeroacoustics. *AIAA J.* **39**, 810–818.

Marble, F. E. & Candel, S. M. 1977 Acoustic disturbance from gas non-uniformities convected through a nozzle. *J. Sound Vib.* **55**, 225–243.

Mayer, D. W. & Paynter, G. C. 1995 Prediction of supersonic inlet unstart caused by freestream disturbances. *AIAA J.* **33**, 266–275.

Poinsot, T. J. & Lele, S. K. 1992 Boundary conditions for direct simulation of compressible viscous flows. *J. Comput. Phys.* **101**, 104–129.

Rein, M., Grabitz, G. & Meier, G. E. A. 1988 Non-linear wave propagation in transonic nozzle flows. *J. Sound Vib.* **122**, 331–346.

Stow, S. R., Dowling, A. P. & Hynes, T. P. 2002 Reflection of circumferential modes in a choked nozzle. *J. Fluid Mech.* **467**, 215–239.

Tam, C. K. W. & Webb, J. C. 1993 Dispersion-relation-preserving finite difference schemes for computational acoustics. *J. Comput. Phys.* **107**, 262–281.

Tsien, H. S. 1952 The transfer functions of rocket nozzles. *Am. Rocket Soc. J.* **22**, 139–143.